Product Release Is Rate-Limiting in the Activation of the Prodrug 5-Fluorocytosine by Yeast Cytosine Deaminase †

ARTICLE *in* BIOCHEMISTRY · MAY 2005

Impact Factor: 3.02 · DOI: 10.1021/bi050095n · Source: PubMed

5 AUTHORS, INCLUDING:

Aizhuo Liu
Michigan State University
24 PUBLICATIONS **1,140** CITATIONS

SEE PROFILE

Product Release Is Rate-Limiting in the Activation of the Prodrug 5-Fluorocytosine by Yeast Cytosine Deaminase†

Lishan Yao,‡,§,|| Yue Li,‡,|| Yan Wu,‡ Aizhuo Liu,‡ and Honggao Yan*,‡

Department of Biochemistry and Molecular Biology and Department of Chemistry, Michigan State University, East Lansing, Michigan 48824

Received January 16, 2005; Revised Manuscript Received February 20, 2005

ABSTRACT: Yeast cytosine deaminase (yCD), a zinc metalloenzyme, catalyzes the hydrolytic deamination of cytosine to uracil. The enzyme is of great biomedical interest because it also catalyzes the deamination of the prodrug 5-fluorocytosine (5FC) to form the anticancer drug 5-fluorouracil (5FU). yCD/5FC is one of the most widely used enzyme/prodrug combinations for gene-directed enzyme prodrug therapy for the treatment of cancers. A pH indicator assay has been developed for the measurement of the steady-state kinetic parameters for the deamination reaction. Transient kinetic studies have shown that the product release is a rate-limiting step in the activation of the prodrug 5FC by yCD. The rate constant of the chemical step for the forward reaction (250 s^{-1}) is ∼8 times that of the product release (31 s^{-1}) and ∼15 times k_{cat} (17 s^{-1}). The transient kinetic results are consistent with those of the steady-state kinetic analysis in the sense that the k_{cat} and K_m values calculated from the rate constants determined by the transient kinetic analysis are in close agreement with those measured by the steady-state kinetic analysis. NMR experiments have demonstrated that free 5FU is in slow exchange with its complex with yCD but has a low affinity for yCD. The transient kinetic and NMR results together suggest that the release of 5FU is rate-limiting in the activation of the prodrug 5FC by yCD and may involve multiple steps.

Yeast cytosine deaminase (yCD),[1] a zinc metalloenzyme, catalyzes the hydrolytic deamination of cytosine to uracil (Scheme 1A). yCD is of great biomedical interest because it also catalyzes the deamination of the prodrug 5-fluorocytosine (5FC, Scheme 1B), which is one of the most widely used prodrugs for gene-directed enzyme prodrug therapy (GDEPT) for the treatment of cancer (*1*, *2*). The challenge in cancer therapy is to kill tumor cells without damaging normal cells. GDEPT meets the challenge by activating a prodrug in the tumor, thereby minimizing damage to normal tissues (*1*, *2*). In cytosine deaminase-based GDEPT, the prodrug 5FC is converted to 5-fluorouracil (5FU) by the enzyme. 5FU is an anticancer drug used to treat breast, colon, rectal, stomach, and pancreatic cancers, and is the drug of choice for treating colorectal carcinoma. However, the drug has high gastrointestinal and hematological toxicities. In contrast, the prodrug 5FC is fairly nontoxic to human, because of the lack of CD activity in human cells. By producing 5FU in the tumor, the CD/5FC system minimizes the undesired toxic effects of 5FU.

Scheme 1

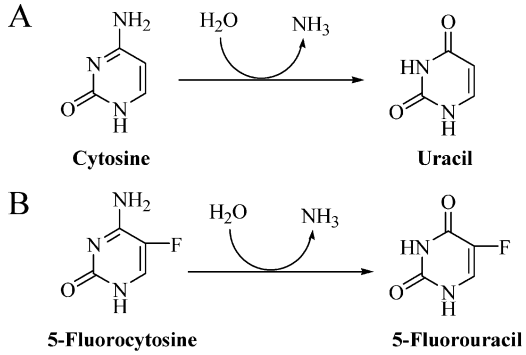

The structure of yCD has been determined recently at high resolution both in the apo form (*3*) and in complex with the inhibitor 2-pyrimidinone, a reaction intermediate analogue (*3*, *4*). The enzyme is a homodimeric enzyme, and the structure of each monomer consists of a central β-sheet flanked by two α-helices on one side and three α-helices on the other. The homodimeric enzyme contains two active centers, and each active center is composed of residues within a single subunit and a catalytic zinc ion coordinated with a histidine (His62), two cysteines (Cys91 and Cys94), and a water molecule in the substrate-free enzyme, the latter serving as a nucleophile in the deamination reaction. The inhibitor is bound in a hydrated adduct [4(*R*)-hydroxyl-3,4-dihydropyrimidine], and the 4-hydroxyl group is coordinated with the catalytic zinc. The bound inhibitor is completely buried,

† This work was supported in part by NIH Grant GM51901 (H.Y.). This study made use of a Varian INOVA 600 NMR spectrometer at Michigan State University funded in part by NSF Grant BIR9512253.

* To whom correspondence should be addressed. Telephone: (517) 353-5282. Fax: (517) 353-9334. E-mail: yanh@msu.edu.

‡ Department of Biochemistry and Molecular Biology.

§ Department of Chemistry.

|| These authors contributed equally to this work.

[1] Abbreviations: 5FC, 5-fluorocytosine; 5FU, 5-fluorouracil; CD, cytosine deaminase; DSS, sodium 2,2-dimethyl-2-silapentane-5-sulfonate; FID, free induction decay; HSQC, heteronuclear single-quantum coherence; IPTG, isopropyl 1-thio-β-D-galactoside; OD, optical density; ONIOM, our own N-layered integrated molecular orbital + molecular mechanics; PAGE, polyacrylamide gel electrophoresis; PCR, polymerase chain reaction; SDS, sodium dodecyl sulfate; TLC, thin-layer chromatography; Tris, 2-amino-2-(hydroxymethyl)-1,3-propanediol; yCD, yeast cytosine deaminase.

10.1021/bi050095n CCC: $30.25
Published on Web 03/25/2005

being covered by a lid composed of Phe114, from the loop between β4 and αD, and Trp152 and Ile156, both from the C-terminal helix. It has been suggested that the C-terminal helix may serve as a "gate" controlling the access to the active center and therefore both substrate binding and product release (*4*). Surprisingly, the structure of apo yCD is essentially the same as that of the inhibitor complex with an rmsd of 0.23 Å for the backbone atoms between the two structures. The active center in the apoenzyme is also covered by the same cluster of hydrophobic residues and appears to be inaccessible to the substrate (*3*). The crystal structure of the apoenzyme also contains a second zinc ion in the substrate binding pocket. However, the noncatalytic zinc is coordinated with water molecules only and has no direct interactions with the protein. The effects of the noncatalytic zinc on the protein structure are not clear. The yCD-catalyzed reaction is believed to proceed via a tetrahedral intermediate with a conserved glutamate (Glu64) serving as a proton shuttle (*3*−*5*).

The catalytic apparatus of yCD, including the catalytic zinc, its coordinated residues, and the proton shuttle, is very similar to that of *Escherichia coli* cytidine deaminase (*3*, *4*), which has been extensively studied (*6*−*8*) and is a paradigm for understanding enzymatic catalysis. yCD has emerged as another excellent model system for studying this class of enzymatic reactions and the role of conformational dynamics in enzymatic catalysis, because high-resolution structures have been determined [1.14 and 1.60 Å for the two structures of the reaction intermediate analogue complex (*3*, *4*) and 1.43 Å for the structure without the reaction intermediate analogue (*3*)]. Furthermore, yCD is only approximately half the size of *E. coli* cytidine deaminase and is amenable to high-resolution NMR analysis, which is being carried out currently in our laboratory.

We are interested in elucidating how yCD catalyzes the activation of the prodrug 5FC to the anticancer drug 5FU and the role of conformational dynamics in the catalysis. In this paper, we show by a combination of transient kinetic and NMR studies that product release is rate-limiting in the activation of the prodrug 5FC by yCD and may involve multiple steps.

EXPERIMENTAL PROCEDURES

Materials. All chemicals and biochemicals were from commercial sources. Cytosine, 5-fluorocytosine, and 5-fluorouracil were purchased from Sigma. [6-^{3}H]-5-Fluorocytosine was purchased from Moravek. [^{15}N]NH_4Cl was purchased from Isotec. Restriction enzymes and T4 ligase were purchased from New England Biolabs. *Pfu* DNA polymerase and the pET-17b vector were purchased from Strategene and Novagen, respectively.

Cloning. The yCD gene was amplified by PCR from yeast genomic DNA. The primers for PCR were 5′-GGG ATC CAT ATG GCA AGC AAG TGG GAT CAG-3′ (forward primer with a *Nde*I site) and 5′-GGA ATT CTA CTC ACC AAT ATC TTC AAA CC-3′ (reverse primer with an *Eco*RI site). The PCR product was digested with *Nde*I and *Eco*RI restriction enzymes and ligated with the vector pET-17b digested with the same restriction enzymes. The ligation mixture was transformed into *E. coli* strain DH5α. The correct coding sequence of the cloned yCD gene was verified by DNA sequencing. The DNA of the expression construct (pET17b-yCD) was then transformed into *E. coli* strain BL21(DE3)pLysS.

Site-Directed Mutagenesis. The W10H mutant was made by PCR-based site-directed mutagenesis. The forward and reverse primers for the mutagenesis were 5′-CATATG-GCAAGCAAGCACGATCAGAAGGGTATGGACATTG-CC-3′ and 5′-GGCAATGTCCATACCCTTCTGATCGT-GCTTGCTTGCCATATG-3′. The mutation was verified by DNA sequencing. The entire gene was sequenced to confirm there was no unintended mutation.

Expression and Purification. Five milliliters of LB medium containing 100 μg/mL ampicillin and 20 μg/mL chloramphenicol was inoculated with a fresh colony of expression strain BL21(DE3)pLysS containing pET17b-yCD. The culture was grown overnight at 33 °C with vigorous shaking (∼200 rpm). The overnight culture was first checked for the expression of yCD by SDS−PAGE and used for seeding a large-scale growth. The expression of yCD was induced by the addition of IPTG to a final concentration of 0.5 mM when the OD_{600} of the culture reached 1.2. The culture was then cooled to room temperature and grown for an additional 6 h. The *E. coli* cells were harvested by centrifugation, washed once with buffer A [50 mM potassium phosphate (pH 7.9)], and kept at −20 °C until they were used.

The frozen bacterial paste was thawed at room temperature and suspended in 100 mL of precooled buffer A. The cells were disrupted with a French press. The resulting lysate was centrifuged for 20 min at ∼27000*g* and 4 °C. Polyethyleneimine was added to the pooled supernatant to a final concentration of 0.1%. The solution was centrifuged immediately after mixing at 15000*g* for 30 min. Ammonium sulfate was added in small portions to the supernatant under constant stirring to 40% saturation. After being stirred for an additional 1 h, the solution was centrifuged at ∼27000*g* for 20 min. The supernatant was loaded onto a phenyl-Sepharose column equilibrated with 40% saturation ammonium sulfate in buffer B [50 mM potassium phosphate (pH 7.0)]. The column was washed with the equilibrium solution until the OD_{280} of the effluent was <0.05 and eluted with a linear ammonium sulfate gradient (from 40 to 0% saturation) in buffer B. Fractions containing yCD were identified by SDS−PAGE and concentrated to ∼15 mL with an Amicon concentrator using a YM10 membrane. The protein solution was then applied to a Sephadex G-75 column equilibrated with 20 mM Tris-HCl (pH 7.5). The column was developed with the same buffer. Fractions from the gel filtration column were monitored by OD_{280} and SDS−PAGE. Pure yCD fractions were pooled and concentrated to 10−20 mL. The concentrated yCD was dialyzed against 2 mM potassium phosphate buffer (pH 7.0) and lyophilized.

^{15}N Labeling. For ^{15}N labeling of yCD, expression strain BL21(DE3)pLysS containing pET17b-yCD was grown in M9 medium with $^{15}NH_4Cl$ as the sole nitrogen source. The cells were grown first at 33 °C and were induced with 0.5 mM IPTG when the culture reached an OD_{600} of 1.2. The culture was further incubated at room temperature for 10 h. The ^{15}N-labeled yCD was purified by the same procedure used for the unlabeled protein.

5-Fluorotryptophan Labeling. To produce 5-fluorotryptophan-labeled yCD, 1 L of M9 medium containing 100 μg/mL ampicillin and 20 μg/mL chloramphenicol was inoculated

with a 5 mL culture of expression strain BL21(DE3)pLysS containing pET17b-yCD and grown overnight at 33 °C with vigorous shaking. The *E. coli* cells were centrifuged and resuspended in 3 L of M9 medium containing 100 μg/mL ampicillin and 20 μg/mL chloramphenicol and grown until the OD_{600} reached 1.0. 5-Fluorotryptophan was then added to a final concentration of 50 mg/L. The culture was incubated further at 33 °C until the OD_{600} reached 1.4 and then induced with 0.5 mM IPTG (final concentration). The cells were harvested by centrifugation after incubation for 4 h at room temperature. The labeled protein was purified, and the percentage of 5-fluorotryptophan labeling was determined by mass spectrometry.

pH Indicator Assay. For measuring the steady-state kinetic parameters of 5FC, the reaction mixture contained 1 mM 5FC, 0.09 mM cresol red, and 8.1−12 μg/mL yCD in 100 mM bicine and 100 mM NaCl (pH 7.5). The reaction was initiated by addition of the enzyme at 25 °C and followed by monitoring the absorption of the pH indicator cresol red at 572 nm. The values of the steady-state kinetic parameters were estimated by the numerical analysis of the time course of the reaction using DYNAFIT (*9*). The steady-state kinetic parameters of cytosine were determined by initial velocity analysis. The reaction mixture contained 0.09 mM cresol red, ~0.6 μg/mL yCD, and 0.2, 0.5, 0.8, 1.2, 2.4, 4.8, or 9.6 mM cytosine. The initial rates were analyzed according to the standard Michaelis−Menten equation.

Stopped-Flow Analysis. Stopped-flow experiments were performed in an Applied Photophysics SX.18MV-R stopped-flow spectrofluorometer at 25 °C. One syringe contained yCD, and the other contained the substrate 5FC. Both yCD and 5FC were dissolved in 20 mM sodium phosphate and 150 mM NaCl (pH 7.3). The absorption at 296 nm was monitored. The data were analyzed by a nonlinear least-squares fit to an exponential equation using Origin (OriginLab).

Quench-Flow Analysis. Quench-flow experiments were carried out with a KinTek RQF-3 rapid quench-flow instrument at 25 °C. All reaction components were dissolved in 20 mM phosphate and 150 mM NaCl (pH 7.3). One syringe contained yCD, and the other contained the substrate 5FC. A trace amount of [6-^{3}H]5FC was used to follow the reactions. The reactions were quenched with 0.5 M acetic acid, 10 mM 5FC, and 10 mM 5FU. The substrate 5FC and product 5FU were separated by TLC on an RP-18 F_{254s} aluminum sheet (Merck) developed with acetonitrite and acetic acid at a 50:1 ratio. After the TLC plate was air-dried for 10 min, 5FC and 5FU were spotted under UV light. The fluorescent spots were cut out and soaked in 1 mL of the developing solution in scintillation vials, and the vials were shaken for 30 min at room temperature. Radioactivities were measured with a Beckman LS6500 scintillation counter after the addition of 7.5 mL of scintillation fluid to each scintillation vial. In pre-steady-state experiments, the reaction mixture contained 20 μM yCD and various concentrations of 5FC. In single-turnover experiments, the reaction mixture contained 300 μM yCD and 15 μM 5FU. All concentrations were those after mixing. The pre-steady-state and single-turnover data were first analyzed by a nonlinear least-squares fit to appropriate single-exponential equations as previously described (*10*). The amplitudes and rate constants were then used to set the initial values for fitting the data to the complete mechanism by numerical analysis using DYNAFIT (*9*).

^{1}H−^{15}N HSQC NMR Spectroscopy. NMR samples were prepared by dissolving ^{15}N-labeled yCD in 100 mM potassium phosphate and 100 μM NaN_3 (pH 7.0) made in H_2O and ^2H_2O (13:1). DSS (20 μM) was used as an internal standard for chemical shift calibration. The initial protein concentration was 1.5 mM in protomers. The NMR samples containing 12 and 20 mM 5FU were made by adding aliquots of a concentrated 5FU solution. The NMR sample containing 75 mM 5FU was made by adding 5FU powder. The sensitivity-enhanced ^{1}H−^{15}N HSQC spectra were acquired at 25 °C on a Varian Inova 600 MHz spectrometer. The spectrum widths were 9476 and 2400 Hz for ^{1}H and ^{15}N dimensions, respectively; 160 (t_1, ^{15}N dimension) × 1946 (t_2, ^{1}H dimension) complex data points were recorded for each spectrum. The number of transients was 32 for each FID with a 1.5 s delay between transients. The NMR data were processed with NMRPipe (*11*).

^{19}F NMR Spectroscopy. ^{19}F NMR experiments were performed on a Varian Inova 300 or 600 MHz NMR spectrometer. The NMR samples were made with the same buffer as that for the ^{1}H−^{15}N HSQC NMR experiments. The NMR spectra were acquired with a spectral width of 5000 Hz, 5000 data points, and 1024 transients for each spectrum with a 2 s delay between transients. The NMR data were processed with VNMR (Varian Associates). The ^{19}F chemical shifts were referenced to $CF_3C_6H_5$.

Saturation transfer experiments were carried out as described by Lian and Roberts (*12*). The NMR sample for the saturation transfer experiments contained 1.5 mM yCD labeled with 5-fluorotryptophan and 24.7 mM 5FU. Two complementary saturation transfer experiments were performed, one saturating a ^{19}F NMR signal of free yCD and the other saturating a ^{19}F NMR signal of 5FU-bound yCD. The signals were saturated with a low-power gated decoupling pulse. The pulse power was set to −2 dB on the basis of the results of preliminary tests. Eight spectra were acquired for each saturation transfer experiment with saturation times of 0, 0.04, 0.06, 0.08, 0.1, 0.12, 0.2, and 0.4 s. The control experiment was performed with the saturation frequency set at one end of the spectrum. The intensity of the monitored peak is described by the following equation.

$$I/I_0 = (k/\lambda)e^{-\lambda t} + R/\lambda$$

where I is the peak intensity of the monitored species when the other species is saturated, I_0 is the peak intensity of the monitored species in the control experiment, k is the rate constant for the conversion of the monitored species to the saturated species, R is the longitudinal relaxation rate constant for the monitored species, and $\lambda = k + R$. The data were fitted by nonlinear least squares regression to an exponential equation using Origin.

$$I_{rel} = Ae^{-\lambda t} + c$$

where I_{rel} is the peak intensity of the monitored species relative to that of the control experiment. When the NMR signal of the bound yCD is saturated, the product of A and λ provides the value for the dissociation rate constant. When the NMR signal of the free yCD is saturated, the product of

A and λ is the rate constant for the conversion of free yCD to bound yCD. The concentrations of the free enzyme, the bound enzyme, and the free ligand can be calculated from the standard equilibrium relationship. The association rate constant can be then obtained because the rate constant for the conversion of free yCD to bound yCD is the product of the association rate constant and the concentration of free 5FU at equilibrium.

RESULTS

Steady-State Kinetic Analysis. CD is traditionally assayed by measuring UV absorbance changes (*13*). Although the method is convenient for routine measurement of CD activity, it is not accurate for measuring kinetic constants, because both the substrate cytosine and the product uracil have high molar extinction coefficients and similar maximum absorbance wavelengths. For example, for an accurate measurement of the K_m value of cytosine (1.1 mM), the substrate concentration must go up to at least 5 mM (~5 times K_m), preferably 10 mM (~10 times K_m). The absorbance for 5 mM cytosine is 30.5 at the maximum absorbance wavelength (267 nm) and 6.1 at the wavelength (286 nm) normally used for measuring CD activity. To overcome this problem, we developed a pH indicator assay. Although the use of pH indicators to monitor the progress of enzymatic reactions has a long history, the technique has not been used for measuring the kinetics of the CD-catalyzed reaction. The pH indicator assay took advantage of the high pK_a (9.25) of ammonia so that essentially all ammonia generated by the CD-catalyzed reaction is converted to ammonium at the assay pH (7.5). The resultant pH change causes a change in the absorbance of the pH indicator at 572 nm. The absorbance change is proportional to the ammonia generated by the CD-catalyzed reaction if the pK_a of the pH indicator is equal to that of the buffer. Cresol red was used as the pH indicator because its pK_a (8.3) matches that of bicine (8.35) used for making the assay buffer. Because kinetic parameters change with pH, the pH changes were kept within 0.05 unit. CO_2 absorption effects were not an issue, because the reaction rates with the amount of the enzyme in the assay were at least 1 order of magnitude higher than the basal rates obtained without the enzyme (control). Therefore, the CO_2 absorption effects could be safely ignored. We also tested the phenol red (pK_a = 7.81) and POPSO (pK_a = 7.82) combination, and the kinetic constants obtained by the two systems were the same. We chose the higher-pK_a system because it gave a higher signal with the same small magnitude of pH change. The buffering capacity was compensated by increasing the concentration of the buffering component. The results of the kinetic measurement by the pH indicator assay are summarized in Table 1. The results showed that yCD has a slightly higher catalytic efficiency (k_{cat}/K_m) for the prodrug 5FC than for the natural substrate cytosine. The catalytic efficiency of yCD for 5FC is ~10-fold higher than that of the *E. coli* enzyme (*14*), in agreement with the report that yCD is a better enzyme for CD/5FC-based GDEPT (*15*).

Transient Kinetic Analysis. To determine the rate constants for the individual steps of the prodrug activation, we performed the transient kinetic analysis of the reaction. We first performed stopped-flow spectrophotometric analysis of the reaction. As shown in Figure 1A, there was a burst increase followed by a steady decrease in absorbance. A similar phenomenon was observed for *E. coli* cytosine deaminase (*14*). The burst increase in absorbance was attributed to the change in the environment of the substrate upon binding to the enzyme, the decrease to the conversion of the substrate to the products. The absorbance changes could be phenomenologically described by an exponential and a linear term. The rate constant of the exponential term is linearly dependent on the concentrations of the substrate (Figure 1B). The apparent association and dissociation rate constants were estimated to be 0.21 μM^{-1} s^{-1} and 33 s^{-1}, respectively, which were probably the low limits because the substrate complex was rapidly converted to the product

Table 1: Kinetic Constants for the Activation of the Prodrug 5FC by yCD[a]

Steady-State Kinetics					
5-fluorocytosine			cytosine		
K_m (mM)	k_{cat} (s^{-1})	k_{cat}/K_m (M^{-1} s^{-1})	K_m (mM)	k_{cat} (s^{-1})	k_{cat}/K_m (M^{-1} s^{-1})
0.16 ± 0.01	17 ± 0.4	1.1×10^5	1.1 ± 0.08	91 ± 4	8.2×10^4

Transient Kinetics						
k_1 (μM^{-1} s^{-1})	k_{-1} (s^{-1})	k_2 (s^{-1})	k_{-2} (s^{-1})	k_3 (s^{-1})	K_m (mM)	k_{cat} (s^{-1})
0.48 ± 0.04	93 ± 20	250 ± 30	91 ± 20	31 ± 2	0.11[b]	21[b]

[a] The steady-state kinetic parameter for cytosine are presented for comparison. [b] K_m and k_{cat} were calculated from the individual rate constants.

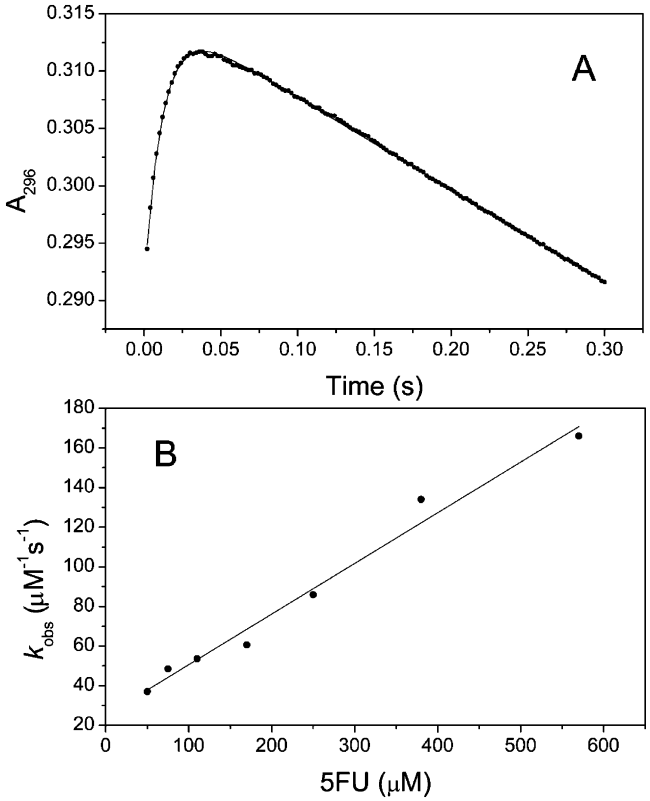

FIGURE 1: Stopped-flow analysis of the activation of the prodrug 5FC by yCD. (A) Time course of the reaction as monitored by OD_{296}. The reaction mixture contained 10 μM yCD and 250 μM 5FC. The solid line was obtained by a nonlinear least-squares fit to an equation with an exponential and a linear term. (B) Linear dependence of the rate constant of the exponential term on the concentration of 5FC.

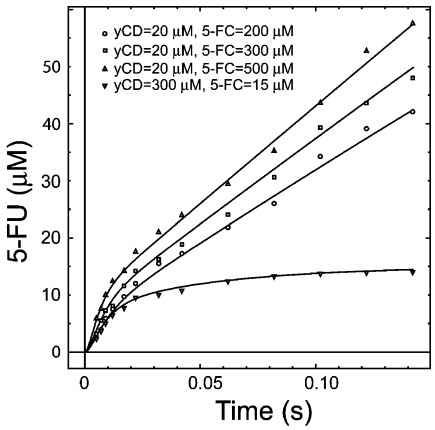

FIGURE 2: Quench-flow analysis of the activation of the prodrug 5FC by yCD. The solid lines were obtained by global fitting using the numerical analysis program DYNAFIT.

complex as shown by a quench-flow analysis.

Because the extinction coefficient of the bound 5FC is slightly higher than that of free 5FC, it was difficult to estimate how much 5FU was formed at the initial phase of the reaction. We then performed several stopped-flow experiments with a pH indicator. It turned out that the data obtained in the first 50 ms were very noisy and unusable. Quench-flow experiments were used instead to obtain definitive kinetic information for the prodrug activation. The results are shown in Figure 2. The burst experiments (the top three lines in Figure 2) clearly indicated that product release is the rate-limiting step in the activation of the prodrug. A single-turnover experiment in which the enzyme concentration was larger than that of the substrate was also performed (the bottom line in Figure 2). The data from both burst and single-turnover experiments were analyzed by global fitting according to the following minimal kinetic mechanism (Scheme 2) using the numerical analysis program DYNAFIT (*9*, *10*). The initial values for the global numerical analysis were obtained by a nonlinear least-squares fit of the data to appropriate exponential equations.

Scheme 2

$$\mathbf{E + S} \underset{k_{-1}}{\overset{k_1}{\rightleftharpoons}} \mathbf{ES} \underset{k_{-2}}{\overset{k_2}{\rightleftharpoons}} \mathbf{EP} \xrightarrow{k_3} \mathbf{E + P}$$

The rate constants obtained by the global numerical analysis are summarized in Table 1. The rate constant for the forward reaction is 8 times that of product release and more than 10 times k_{cat}. The K_m and k_{cat} values calculated from the individual rate constants were very similar to those determined by steady-state kinetic measurements, indicating that the individual rate constants determined by the transient kinetic analysis are consistent with the steady-state kinetic parameters. The slow product release is probably due to the slow dissociation of 5FU and was confirmed by the NMR analysis of the binding of 5FU to yCD.

NMR Analysis. To confirm that the product release is rate-limiting in the prodrug activation, several NMR experiments were performed. First, we acquired $^1H-^{15}N$ HSQC spectra of ^{15}N-labeled yCD in the absence of 5FU and in the presence of 12, 20, and 80 mM 5FU. As shown in Figure 3B, many residues had two sets of cross-peaks under unsaturated conditions, indicating that 5FU was in slow exchange with

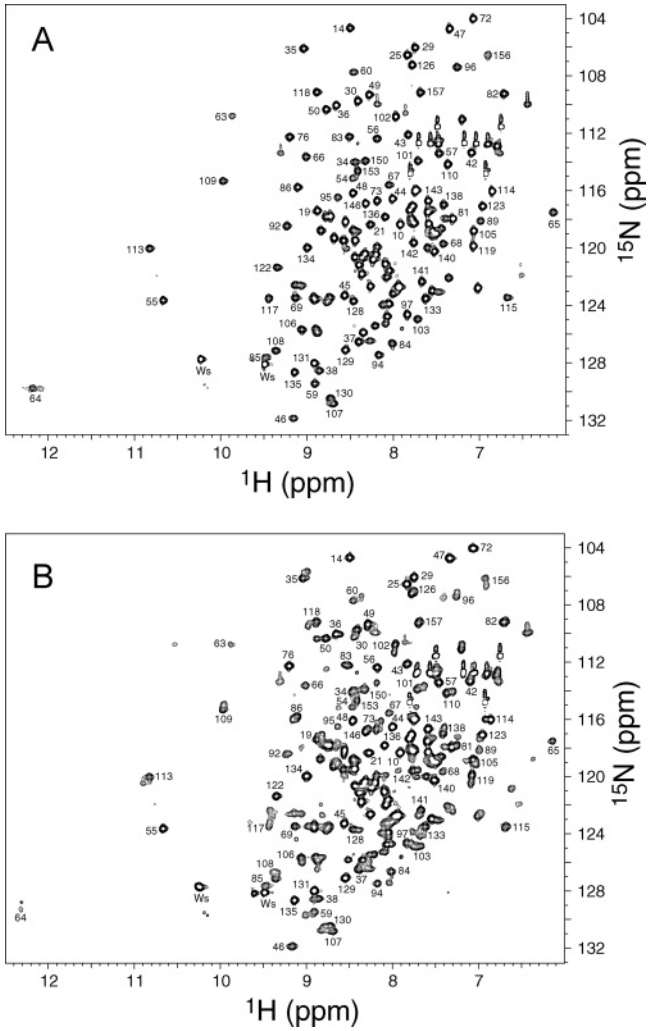

FIGURE 3: $^1H-^{15}N$ HSQC spectra of yCD. Sequential assignments are indicated with residue numbers: (A) 1.5 mM yCD and (B) 1.5 mM yCD with 12 mM 5FU.

the complex of yCD and 5FU on the NMR time scale and yCD was not saturated with 5FU. Only one set of HSQC cross-peaks were obtained when the 5FU concentration reached ~80 mM (the maximum solubility), indicating that yCD was predominately in the bound form at this 5FU concentration (data not shown). The sequential resonance assignment of yCD in complex with the reaction intermediate analogue 5-fluoro-2-pyrimidinone has been achieved by three-dimensional (3D) double- and triple-resonance NMR experiments, including ^{15}N-edited 3D NOESY, HNCA, HN(CO)CA, HN(CA)CB, HN(COCA)CB, HNCO, HN(CA)CO, HCCH-TOCSY, C(CO)NH-TOCSY, and H(CCO)NH-TOCSY data (*16*), using singly, doubly, and triply labeled yCD samples (L. Yao et al., unpublished results). Because most of the cross-peaks in the HSQC spectra are well resolved, many cross-peaks of unliganded yCD (Figure 3A) and its complex with 5FU (Figure 3B) could be assigned by comparison with the assigned $^1H-^{15}N$ HSQC spectrum of yCD in complex with the reaction intermediate analogue. Most of the cross-peaks that moved upon the binding of 5FU belong to the residues in the vicinity of the active site. The K_d of the binary product complex was estimated to be ~20 mM, because about equal amounts of yCD were in the free form and the bound form at 20 mM 5FU. Second, we acquired ^{19}F NMR spectra of 5FU free and in complex with

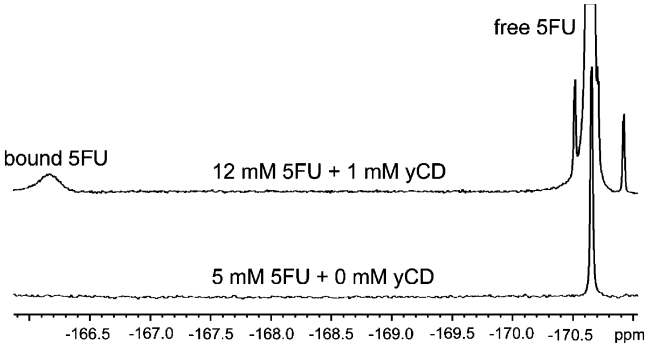

FIGURE 4: ^{19}F NMR spectra of free (unbound) 5FU and the yCD-bound 5FU. The smaller peaks near the strong peak of free 5FU in the top spectrum are ^{13}C satellite peaks.

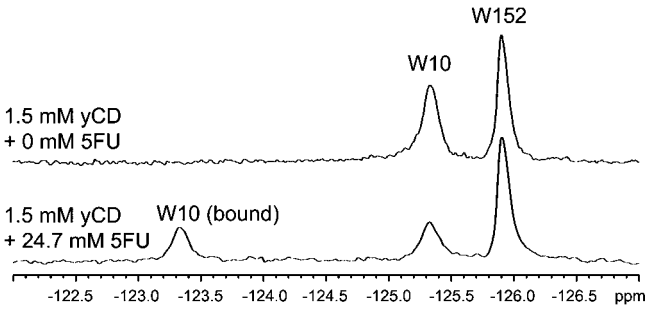

FIGURE 5: ^{19}F NMR spectra of yCD labeled with 5-fluorotryptophan: (A) 1.5 mM 5-fluorotryptophan-labeled yCD and (B) 1.5 mM 5-fluorotryptophan-labeled yCD with 24.7 mM 5FU.

yCD (Figure 4). The formation of the yCD complex shifted the ^{19}F NMR signal of 5FU by ~4.5 ppm. The results clearly indicated that the free 5FU is in slow exchange with the yCD and 5FU complex on the ^{19}F NMR time scale. Third, we acquired ^{19}F NMR spectra of yCD labeled with 5-fluorotryptophan in the absence and presence of 5FU (Figure 5). The degree of 5-fluorotryptophan labeling was estimated to be ~90% on the basis of the ^{1}H−^{15}N HSQC spectra of singly (^{15}N) yCD and doubly labeled (^{15}N and ^{19}F) yCD proteins. The k_{cat} and K_m values of the ^{19}F-labeled yCD were 15 ± 0.4 s^{-1} and 80 ± 6 μM, respectively, indicating that the 5-fluorotryptophan labeling has no significant effects on the kinetic properties of yCD. The ^{19}F-labeled yCD exhibited two ^{19}F NMR peaks, and one was much sharper than the other. The binding of 5FU shifted the broader NMR peak by ~2 ppm but caused no significant change in the position of the narrower peak (Figure 5). The wild-type yCD has two tryptophan residues, Trp10 at the N-terminus (away from the active site) and Trp152 at the active site. The two ^{19}F NMR peaks were assigned on the basis of the comparison with the ^{19}F NMR spectrum of the yCD mutant W10H, which showed only one peak from Trp152 (data not shown). Surprisingly, the shifted peak belonged to Trp10 at the N-terminus rather than Trp152 at the active site. The result again indicated that 5FU is in slow exchange with its complex with the enzyme on the NMR time scale. Furthermore, the intensities of free yCD and bound yCD were approximately equal in the presence of 24.7 mM 5FU, again indicating that the K_d value for the binary complex is ~20 mM. Fourth, we determined the exchange rate constants by NMR saturation transfer experiments. The results are shown in Figure 6. The results were analyzed using a simple one-step binding model. The dissociation rate constant was

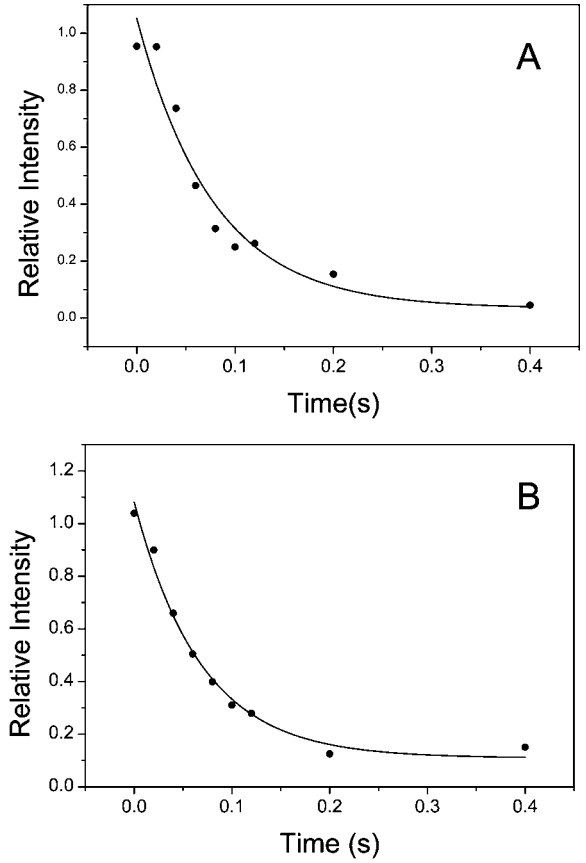

FIGURE 6: NMR saturation transfer analysis of the binding of 5FU to the 5-fluorotryptophan-labeled yCD. The NMR sample contained 1.5 mM 5-fluorotryptophan-labeled yCD and 24.7 mM 5FU. The data in panels A and B were obtained by irradiating the ^{19}F NMR nuclei of the bound and free yCD, respectively. The solid lines were obtained by a nonlinear least-squares fit of the data as described in Experimental Procedures.

determined by saturating the ^{19}F NMR signal of the bound yCD, which was 13 s^{-1}. The rate for the formation of the complex, a product of the association rate constant and the concentration of free 5FU at equilibrium, was determined by saturating the ^{19}F NMR signal of free yCD, which was 14 s^{-1}. The concentration of free 5FU was calculated to be 24 mM using the standard equilibrium relationship. The association rate constant therefore was 0.6 mM^{-1} s^{-1}, and the K_d was 22 mM. The results indicated that 5FU is in slow exchange with its yCD complex but has a rather high K_d.

DISCUSSION

yCD is of great biomedical interest because it catalyzes the deamination of the prodrug 5FC to form the anticancer drug 5FU. By a combination of transient kinetic and NMR studies, we have clearly shown that product release is a rate-limiting step in the activation of the prodrug 5FC by yCD. The transient kinetic studies showed that the rate constant of the chemical step for the forward reaction (250 s^{-1}) is ~8 times that of the product release (31 s^{-1}) and ~15 times k_{cat} (17 s^{-1}). The transient kinetic results are consistent with those of the steady-state kinetic analysis in the sense that the k_{cat} and K_m values calculated from the rate constants determined by the transient kinetic analysis are in close agreement with those measured by the steady-state kinetic analysis. The steady-state kinetic parameters, however, are

insufficient for the description of the kinetics of the prodrug activation. The yCD-catalyzed activation of the prodrug 5FC generates two products, 5FU and ammonia. The four NMR experiments described in the Results clearly indicated that the release of 5FU is rate-limiting in the activation of the prodrug 5FC by yCD.

There are two possible causes for the slow release of 5FU by yCD. One involves the breaking of the coordination between 5FU and the catalytic zinc, and the other involves the opening of the lid that covers the active site. When 5FC is converted to 5FU at the active site of yCD, the oxygen at position 4 of 5FU is coordinated with the catalytic zinc. Using the ONIOM methodology (*17*−*24*), our recent computational study of the deamination of cytosine showed that, energetically, the cleavage of the O4−Zn bond is rather difficult either in the presence or in the absence of ammonia (*5*). The computational study suggests that uracil is liberated from the zinc by an oxygen exchange mechanism that involves the formation of a *gem*-diol intermediate from the Zn-bound uracil and a water molecule, cleavage of the C4−O^{Zn} bond, and the regeneration of the Zn-coordinated water. The rate-determining step in oxygen exchange is the formation of the *gem*-diol intermediate, which is also the rate-determining step for the overall yCD-catalyzed deamination reaction.

5FU is also likely to be completely buried at the active site of yCD. The structure of yCD in complex with the reaction intermediate analogue 2-pyrimidinone has been determined recently at high resolution (*3*, *4*). The bound reaction intermediate analogue is completely buried, being covered by a lid composed of Phe114, Trp152, and Ile156, the latter two of which are from the C-terminal helix. It is possible that the opening of the lid may also determine the rate of product release in yCD. Furthermore, the structure of apo yCD is essentially the same as that of the reaction intermediate complex (*3*). The active center is also covered by the same cluster of hydrophobic residues in the apoenzyme and appears to be inaccessible to the substrate (*3*). It appears that the opening of the lid is required for not only product release but also substrate binding. Thus, the release or binding of 5FU may involve multiple steps as illustrated in Scheme 3, where E^o and E^c represent the open and closed conformations of the unliganded enzyme, respectively, E^c−5FU is a complex in which 5FU is coordinated with the catalytic zinc and yCD is in a closed conformation, E^c·5FU is a complex in which 5FU is not coordinated with the zinc and the enzyme is still in a closed conformation, and E^o·5FU is a complex in which 5FU is not coordinated with the zinc but the enzyme is in an open conformation.

Scheme 3

$$E^c\text{-}5FU \rightleftharpoons E^c.5FU \rightleftharpoons E^o.5FU \rightleftharpoons E^o \rightleftharpoons E^c$$

The NMR results are interesting, because the results not only showed that the release of 5FU is a slow step in the deamination of 5FC but also showed that 5FU has a low affinity for yCD (high K_d). In general, slow exchange means tight binding and a low K_d. One explanation for the high K_d is that yCD exists in two conformations, a closed conformation with an inaccessible active center and an open conformation with an accessible active center, as illustrated in Scheme 3. 5FU binds to the open conformation only. The equilibrium is in favor of the closed conformation, which is most populated and was crystallized (*3*). The apparent K_d is the reciprocal of the overall equilibrium constant, which is a product of the equilibrium constant for the conformational transition of the unliganded yCD and the equilibrium constant for the binding of 5FU to the open conformation. An equilibrium constant in favor of the closed conformation will increase the apparent K_d by a factor of the reciprocal of the equilibrium constant. The unusually low apparent association rate constant may also be attributed to the multiple-step nature of the binding of 5FU to yCD.

yCD belongs to the CDA family of purine/pyrimidine deaminases (*3*, *4*). In addition to yCD and other fungal cytosine deaminases, members of the family of enzymes include cytidine deaminases, guanine deaminases, and riboflavin biosynthesis enzymes. These enzymes have similar structures with a zinc-containing catalytic apparatus (*25*). The structures of the family of enzymes reported to date are all in a closed conformation. Because these enzymes all have a closed conformation and most likely follow a similar chemical mechanism, product release may also be rate-limiting in the reactions catalyzed by other members of this family of enzymes. However, a lack of viscosity dependence on the k_{cat} of *E. coli* cytidine deaminase suggests that product release may not be rate-limiting in the reaction catalyzed by the enzyme (*26*). On the other hand, full ^{15}N kinetic isotope effects are manifested in the reaction catalyzed by mutants with significantly reduced catalytic efficiencies but not the wild-type cytidine deaminase (*7*), indicating that there is another step influencing the rate besides the slow C^4−N^4 bond cleavage in the deamination of cytidine.

In conclusion, the transient kinetic and NMR data together clearly showed that the release of 5FU is rate-limiting in the activation of the prodrug 5FC by yCD and may involve multiple steps, the interconversion of yCD between a closed and an open conformation and the cleavage or formation of the coordination between 5FU and the catalytic zinc of yCD.

REFERENCES

1. Aghi, M., Hochberg, F., and Breakefield, X. O. (2000) Prodrug activation enzymes in cancer gene therapy, *J. Gene Med. 2*, 148−164.
2. Greco, O., and Dachs, G. U. (2001) Gene directed enzyme/prodrug therapy of cancer: Historical appraisal and future prospectives, *J. Cell. Physiol. 187*, 22−36.
3. Ireton, G. C., Black, M. E., and Stoddard, B. L. (2003) The 1.14 Å crystal structure of yeast cytosine deaminase evolution of nucleotide salvage enzymes and implications for genetic chemotherapy, *Structure 11*, 961−972.
4. Ko, T.-P., Lin, J.-J., Hu, C.-Y., Hsu, Y.-H., Wang, A. H.-J., and Liaw, S.-H. (2003) Crystal structure of yeast cytosine deaminase. Insights into enzyme mechanism and evolution, *J. Biol. Chem. 278*, 19111−19117.
5. Sklenak, S., Yao, L. S., Cukier, R. I., and Yan, H. G. (2004) Catalytic mechanism of yeast cytosine deaminase: An ONIOM computational study, *J. Am. Chem. Soc. 126*, 14879−14889.
6. Schramm, V. L., and Bagdassarian, C. K. (1999) Deamination of nucleosides and nulceotides and related reactions, in *Enzymes, Enzyme Mechanisms, Proteins, and Aspects of NO Chemistry* (Poulter, C. D., Ed.) pp 71−100, Elsevier: Amsterdam.
7. Snider, M. J., Reinhardt, L., Wolfenden, R., and Cleland, W. W. (2002) ^{15}N kinetic isotope effects on uncatalyzed and enzymatic deamination of cytidine, *Biochemistry 41*, 415−421.
8. Snider, M. J., Lazarevic, D., and Wolfenden, R. (2002) Catalysis by entropic effects: The action of cytidine deaminase on 5,6-dihydrocytidine, *Biochemistry 41*, 3925−3930.

9. Kuzmic, P. (1996) Program DYNAFIT for the analysis of enzyme kinetic data: Application to HIV proteinase, *Anal. Biochem. 237*, 260−273.
10. Li, Y., Gong, Y., Shi, G., Blaszczyk, J., Ji, X., and Yan, H. (2002) Chemical transformation is not rate-limiting in the reaction catalyzed by *Escherichia coli* 6-hydroxymethyl-7,8-dihydropterin pyrophosphokinase, *Biochemistry 41*, 8777−8783.
11. Delaglio, F., Grzesiek, S., Vuister, G. W., Zhu, G., Pfeifer, J., and Bax, A. (1995) NMRPipe: A multidimensional spectral processing system based on UNIX pipes, *J. Biomol. NMR 6*, 277−293.
12. Lian, L. Y., and Roberts, G. C. K. (1993) Effects of chemical exchange on NMR spectra, in *NMR of Macromolecules* (Roberts, G. C. K., Ed.) IRL Press, New York.
13. Ipata, P. L., Marmocchi, F., Magni, G., and Felicioli, R. (1971) Baker's yeast cytosine deaminase. Some properties and allosteric inhibition by nucleosides and nucleotides, *Biochemistry 10*, 4270−4276.
14. Porter, D. J. T. (2000) *Escherichia coli* cytosine deaminase: The kinetics and thermodynamics for binding of cytosine to the apoenzyme and the Zn^{2+} holoenzyme are similar, *Biochim. Biophys. Acta 1476*, 239−252.
15. Kievit, E., Bershad, E., Ng, E., Sethna, P., Dev, I., Lawrence, T. S., and Rehemtulla, A. (1999) Superiority of yeast over bacterial cytosine deaminase for enzyme/prodrug gene therapy in colon cancer xenografts, *Cancer Res. 59*, 1417−1421.
16. Gardner, K. H., and Kay, L. E. (1998) The use of ^{2}H, ^{13}C, ^{15}N multidimensional NMR to study the structure and dynamics of proteins, *Annu. Rev. Biophys. Biomol. Struct. 27*, 357−406.
17. Dapprich, S., Komaromi, I., Byun, K. S., Morokuma, K., and Frisch, M. J. (1999) A new ONIOM implementation in Gaussian98. Part I. The calculation of energies, gradients, vibrational frequencies and electric field derivatives, *J. Mol. Struct. 462*, 1−21.
18. Humbel, S., Sieber, S., and Morokuma, K. (1996) The IMOMO method: Integration of different levels of molecular orbital approximations for geometry optimization of large systems: Test for *n*-butane conformation and S_N2 reaction: RCl + Cl, *J. Chem. Phys. 105*, 1959−1967.
19. Kuno, M., Hannongbua, S., and Morokuma, K. (2003) Theoretical investigation on nevirapine and HIV-1 reverse transcriptase binding site interaction, based on ONIOM method, *Chem. Phys. Lett. 380*, 456−463.
20. Svensson, M., Humbel, S., Froese, R. D. J., Matsubara, T., Sieber, S., and Morokuma, K. (1996) ONIOM: A multilayered integrated MO+MM method for geometry optimizations and single point energy predictions. A test for Diels−Alder reactions and $Pt(P(t\text{-}Bu)_3)_2 + H_2$ oxidative addition, *J. Phys. Chem. 100*, 19357−19363.
21. Svensson, M., Humbel, S., and Morokuma, K. (1996) Energetics using the single point IMOMO (integrated molecular orbital plus molecular orbital) calculations: Choices of computational levels and model system, *J. Chem. Phys. 105*, 3654−3661.
22. Vreven, T., Mennucci, B., da Silva, C. O., Morokuma, K., and Tomasi, J. (2001) The ONIOM-PCM method: Combining the hybrid molecular orbital method and the polarizable continuum model for solvation. Application to the geometry and properties of a merocyanine in solution, *J. Chem. Phys. 115*, 62−72.
23. Vreven, T., and Morokuma, K. (2000) On the application of the IMOMO (integrated molecular orbital plus molecular orbital) method, *J. Comput. Chem. 21*, 1419−1432.
24. Vreven, T., Morokuma, K., Farkas, O., Schlegel, H. B., and Frisch, M. J. (2003) Geometry optimization with QM/MM, ONIOM, and other combined methods. I. Microiterations and constraints, *J. Comput. Chem. 24*, 760−769.
25. Liaw, S. H., Chang, Y. J., Lai, C. T., Chang, H. C., and Chang, G. G. (2004) Crystal structure of *Bacillus subtilis* guanine deaminase: The first domain-swapped structure in the cytidine deaminase superfamily, *J. Biol. Chem. 279*, 35479−35485.
26. Snider, M. J., Gaunitz, S., Ridgway, C., Short, S. A., and Wolfenden, R. (2000) Temperature effects on the catalytic efficiency, rate enhancement, and transition state affinity of cytidine deaminase, and the thermodynamic consequences for catalysis of removing a substrate "anchor", *Biochemistry 39*, 9746−9753.

BI050095N